

Iron Single Atom Catalyzed Quinoline Synthesis

Zhongxin Chen, Jingting Song, Xinwen Peng,* Shibo Xi, Jia Liu, Wenhui Zhou, Runlai Li, Rile Ge, Cuibo Liu, Haisen Xu, Xiaoxu Zhao, Haohan Li, Xin Zhou, Lu Wang, Xing Li, Linxin Zhong, Alexandre I. Rykov, Junhu Wang, Ming Joo Koh, and Kian Ping Loh*

The production of high-value chemicals by single-atom catalysis is an attractive proposition for industry owing to its remarkable selectivity. Successful demonstrations to date are mostly based on gas-phase reactions, and reports on liquid-phase catalysis are relatively sparse owing to the insufficient activation of reactants by single-atom catalysts (SACs), as well as, their instability in solution. Here, mechanically strong, hierarchically porous carbon plates are developed for the immobilization of SACs to enhance catalytic activity and stability. The carbon-based SACs exhibit excellent activity and selectivity (~68%) for the synthesis of substituted quinolines by a three-component oxidative cyclization, affording a wide assortment of quinolines (23 examples) from anilines and acetophenones feedstock in an efficient, atom-economical manner. Particularly, a Cavosonstat derivative can be synthesized through a one-step, Fe₁-catalyzed cyclization instead of traditional Suzuki coupling. The strategy is also applicable to the deuteration of quinolines at the fourth position, which is challenging by conventional methods. The synthetic utility of the carbon-based SAC, together with its reusability and scalability, renders it promising for industrial scale catalysis.

has seen limited progress owing to their instability in solution and insufficient activation of reactants by single metal sites under ambient conditions.^[4,5] Consequently, applications of SACs in organic synthesis were limited to certain hydrogenations,^[6,7] oxidations,^[8,9] and C–C bond formations.^[10] Very recently, we have reported the first SAC-catalyzed preparation of pharmaceuticals (Lonidamine etc., and their ¹⁵N-labeled analogues) by selective hydrogenation to *E*-hydrazones and subsequent cyclization using Pt₁/CeO₂ catalyst.^[11] We have also developed the late-stage functionalization of pharmaceuticals (Tamiflu) by chemoselective oxidation of sulfides using Co₁-in-MoS₂ catalyst.^[12] Despite excellent functional group tolerance and synthetic utility in both cases, the scope is limited by the use of complex starting materials (i.e., carboxylic esters mediated α -diazoesters synthesis and multifunctionalized sulfides), and the

inaccessibility to synthesize multi-ring system as the reactions mainly involve simple hydrogenation/oxidation.^[11,12]

Quinolines, a major class of heterocycles, are widely occurring in natural and synthetic products with diverse pharmacological and physical properties.^[13,14] Among the many methods to synthesize quinolines, the classical Friedländer condensation of an aromatic 2-amino-substituted carbonyl compound with another substituted carbonyl derivative is one of the simplest

1. Introduction

The past decade has witnessed an explosion of research in single-atom catalysts (SACs) on account of their maximized atom utilization efficiency, remarkable turnover frequency, and selectivity in gas-phase reactions and (photo)electrocatalysis.^[1–3] Despite the advances in gas-phase reactions, the liquid-phase transformation of chemicals into high-value products by SACs

Dr. Z. Chen, J. Song, Dr. J. Liu, Prof. R. Li, Prof. C. Liu, Prof. H. Xu, Dr. X. Zhao, H. Li, Dr. X. Zhou, L. Wang, Dr. X. Li, Prof. M. J. Koh, Prof. K. P. Loh
Department of Chemistry
3 Science Drive 3, Singapore 117543, Singapore
E-mail: chmlhkp@nus.edu.sg

J. Song, L. Wang, Prof. K. P. Loh
Joint School of National University of Singapore and Tianjin University
International Campus of Tianjin University
Binhai New City, Fuzhou 350207, China

Prof. X. Peng, Prof. L. Zhong
State Key Laboratory of Pulp and Paper Engineering
South China University of Technology
Guangzhou 510641, China
E-mail: fexwpeng@scut.edu.cn

 The ORCID identification number(s) for the author(s) of this article can be found under <https://doi.org/10.1002/adma.202101382>.

Dr. S. Xi
Institute of Chemical and Engineering Sciences
Agency for Science, Technology and Research (A*STAR)
1 Pesek Road, Jurong Island, Singapore 627833, Singapore

W. Zhou, Dr. R. Ge, Prof. A. I. Rykov, Prof. J. Wang
Center for Advanced Mössbauer Spectroscopy
Dalian Institute of Chemical Physics
Chinese Academy of Sciences
Dalian, Liaoning 116023, China

Prof. C. Liu
Department of Chemistry
Institute of Molecular Plus
School of Science
Tianjin University
Tianjin 300072, China

DOI: 10.1002/adma.202101382

and most effective approaches.^[13,14] Owing to the requirement for specialized substrates (ortho-substituted aniline) and the lack of multifunctional capability, researchers have devised the three-component annulation reaction of readily available materials, including transition metal-catalyzed Povarov reaction using arylamine, aldehyde, and a third component (alkene, alkyne, etc.).^[15,16] The conundrum is that homogeneous reactions usually entail tedious separation of catalyst residues, whereas the use of heterogeneous catalysts leads to undesired side reactions.^[17,18] There is therefore a compelling need to develop SACs that enable efficient access to valuable quinoline derivatives with high selectivity and are easily separable from the reaction mixtures.

Since conventional liquid phase reactions are limited by high activation energy for the activation of reactants,^[1–3,19] a hierarchically structured support for SAC is favorable for high turnover frequency by maximizing the exposure of metallic sites to reactants. However, the preparation of SAC usually requires a pyrolysis step, which inevitably collapses the pores or channels in the porous support supporting the SAC.^[1,20] Natural wood possesses abundant channels and can be utilized as a mechanically robust scaffold for constructing hierarchically porous support for catalysts via scalable top-down approaches.^[21–23] Using natural woods with built-in channels is cost-effective and convenient compared to bottom-up synthesis of hierarchical scaffolds from molecular precursors.^[24] This allows direct fabrication of catalyst body without the addition of porogens, binders, fillers, or other additives.^[25] We have previously demonstrated the capability of nitrogen-doped carbonized wood plate as a monolithic, “breathable” cathode for Zn–air batteries.^[26,27] In this regard, natural wood with excellent mechanical stability and abundant built-in channels can be a good candidate as cost-effective, scalable scaffold.

Herein, we report the construction of a robust SACs platform by immobilizing metal ion precursors in natural wood, following by the carbonization to convert into stable SACs. The carbon-based SACs was processed to optimize the metal–N₄

coordination (metal = Fe, Co, Ni, or Cu), which was found to exhibit excellent activity and selectivity (≈68%) for three-component oxidative cyclization to synthesize 6-methoxy-2-phenylquinoline, outperforming the benchmark Pd/C, Fe/C, and homogeneous FeCl₃ catalysts. Density functional theory (DFT) calculations show that the Fe–N₄ coordination centers present lower reaction barriers to condensation and product desorption than Fe–C₂N₂ and Fe–C₁N₃ catalytic centers, thus affording a higher reaction efficiency.

2. Results

2.1. Carbon-Based, Hierarchically Porous Single-Atom Catalysts

We have employed a modified top-down approach as shown in **Figure 1** to immobilize SAC on hierarchically porous carbons. Natural birch wood was treated with metal ion precursors (FeCl₃, CoCl₂, NiCl₂, or CuCl₂) by a similar pretreatment process in pulp and paper industry to form a black liquor. During this pretreatment, metal ions will strongly bind to the oxygenated groups in lignin and break the β-O-4 ether bonds.^[28–30] The hydrothermal treated wood was then carbonized at high temperature with extrinsic nitrogen source (urea) to convert into stable SACs (denoted as Fe-T SACs where T represents the pyrolysis temperature). The addition of N source (urea) is vital to the SAC preparation because significant metal particle aggregation is observed in the control sample without urea in **Figure S2**, Supporting Information. Such top-down process is highly scalable, producing >20 g of carbon-based SACs with 0.8 wt% of metal in a single batch experiment. The hierarchically porous SAC is also mechanically strong, supporting > 50 times of its weight in **Figure S1**, Supporting Information.

We first examined the morphology of such carbon-based SACs by scanning electron microscopy (SEM). As shown in **Figure 2A** and **Figure S3**, Supporting Information, natural birch wood has a highly orientated macroporous structure

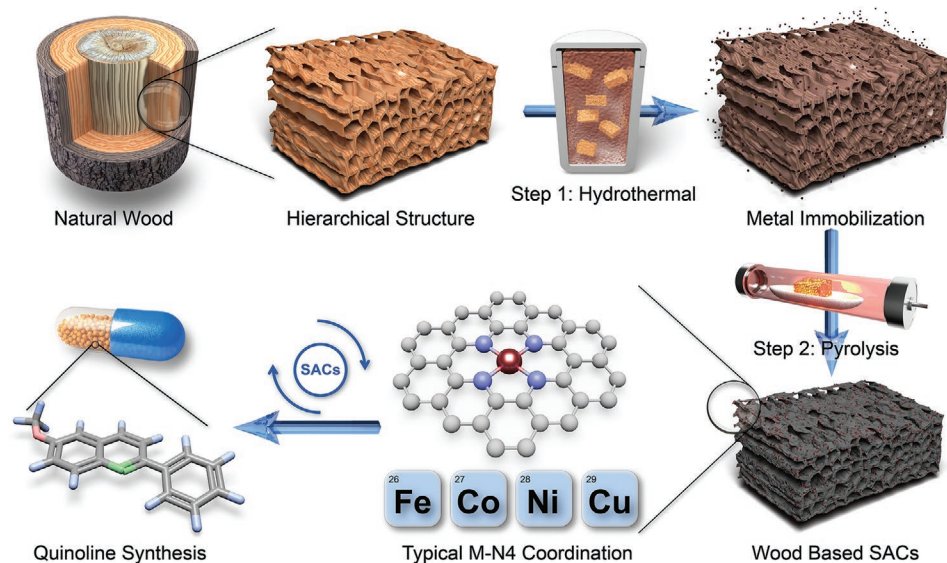


Figure 1. Schematic of the preparation of carbon-based single-atom catalysts.

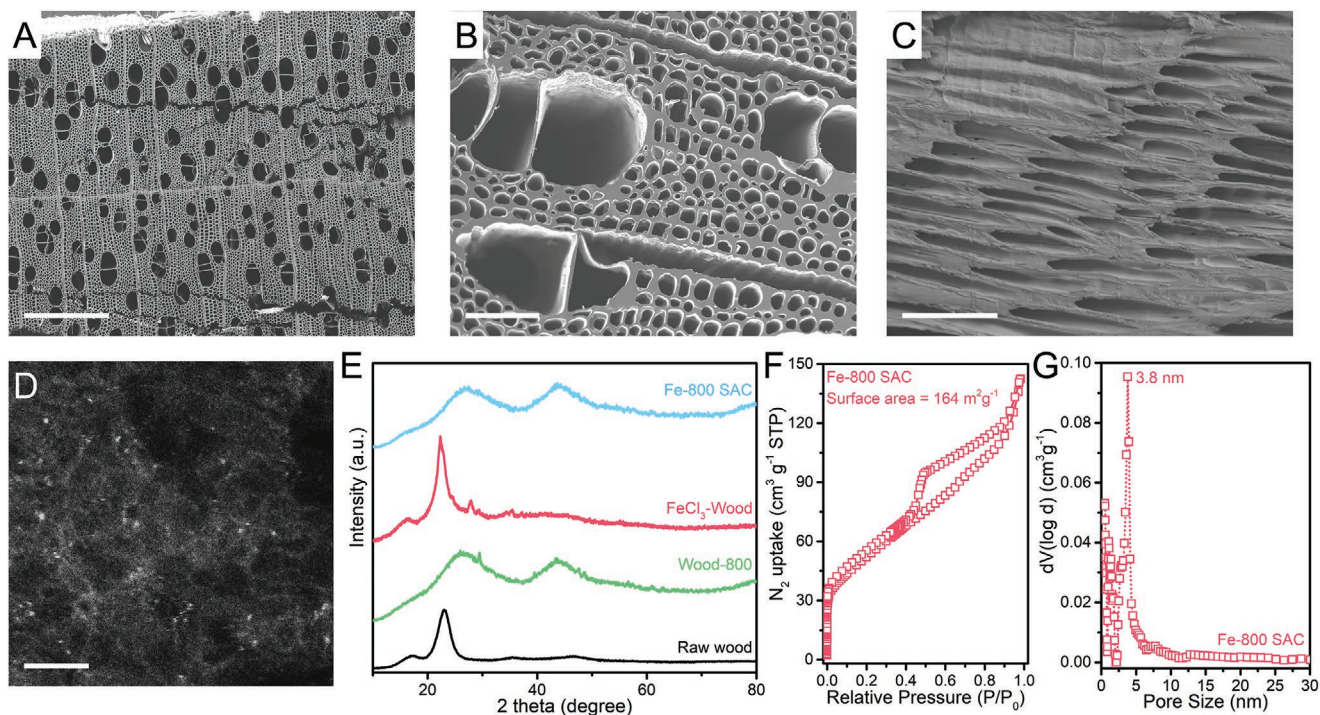


Figure 2. Hierarchically porous structure of Fe-800 SAC. A,B) SEM images showing the macroporous channels of: A) raw wood and B) Fe-800 SAC along the vertical direction. C) SEM image of Fe-800 SAC along the parallel direction. D) Atomic-resolution STEM-HAADF image of Fe-800 SAC. E) XRD patterns of various samples. F) N₂ adsorption/desorption isotherm at 77 K and G) pore-size distribution of Fe-800 SAC. Scale bars: A) 500 μm ; B,C) 50 μm ; D) 2 nm.

with most of the macropores having diameters of 10–20 μm from its aligned cellulose fibers and some macropores with >100 μm from its vessels. Such hierarchically porous structure is beneficial for the diffusion of liquid into the inner cell walls.^[31] The hydrothermal treatment and pyrolysis processes did not affect the intrinsic macropores, which were well-retained in Figure 2B,C and Figures S4–S6, Supporting Information. Apart from the macroporous structure, Fe-800 SAC exhibits a typical type-IV behavior with a Brunauer–Emmett–Teller (BET) surface area of 164 m² g⁻¹ and a prominent pore size of 3.8 nm in the N₂ gas adsorption/desorption isotherms in Figure 2F,G. The presence of uniformly distributed N and Fe on the carbon skeleton was confirmed by elemental mapping in Figure S7, Supporting Information. The N and Fe mass loading were determined as 7.3–4.4% and 0.6–0.8% by elemental analysis (EA) and inductively coupled plasma (ICP) at various pyrolysis temperatures in Table S1, Supporting Information. The atomic dispersion of transition metal in wood-derived catalysts was characterized by scanning transmission electron microscopy in annular dark-field mode (STEM-ADF). Because of abundant N ligands, transition metal single atoms such as Fe₁, Co₁, Ni₁, or Cu₁ can be readily immobilized on the carbonized plates,^[29] whose uniform distribution is observed as bright spots in Figure 2D and Figures S8 and S9. The doping configuration of N is also verified by X-ray photoelectron spectroscopy (XPS) in Figure S12. Two characteristic peaks at 398.5 and 400.8 eV can be assigned to the pyridinic N and graphitic N, respectively.^[26,32] The presence of defective sites and functional groups for the immobilization of single atom is further confirmed by Raman, Fourier

transform infrared (FT-IR), and solid-state NMR spectra in Figure S10–S13, Supporting Information.

The electronic and coordination structure of iron in carbon-based SAC were validated by X-ray absorption near-edge structure (XANES) and extended X-ray absorption fine structure (EXAFS).^[33,34] The Fe K-edge XANES spectrum of Fe-800 SAC exhibits a white line intensity similar to iron phthalocyanine (FePc) in Figure 3A, indicating an oxidation state of +2 after in situ reduction by pyrolysis. This is supported by a comprehensive analysis on the pre-edge feature, edge location and white line intensity in Figure S14 and Table S2, Supporting Information, as well as, Fe_{2p} XPS and Fe L_{2,3}-edge XAS spectra in Figure S12, Supporting Information. Both calculated and experimental XANES curves in Figure 3B and Figure S15, Supporting Information, confirms a pyridinic type Fe–N₄ structure in our samples, where Fe–C₁N₃ and Fe–C₂N₂ species may co-exist.^[11,35] Other typical Fe–N–C structures is excluded due to mismatch of the simulation and experiment. Unlike typical signals of FeCl₃, the Fourier-transformed EXAFS spectrum of FeCl₃-wood exhibits a prominent Fe–O peak at ≈ 1.53 \AA in Figure 3C. This is a result of transformation of the iron salt to Fe–O during hydrothermal treatment. Fe-800 SAC also exhibits a characteristic Fe–N peak at 1.44 \AA , which is fitted with a coordination number of 4 in Table S3, Supporting Information. No metallic Fe–Fe peak at 2.21 \AA is observed for Fe-800 SAC, revealing that Fe₁ exists as isolated single atoms in carbon-based SACs, consistent with the HAADF-STEM images and the absence of a metal particle peak at $\approx 44^\circ$ in the XRD spectrum. Wavelet transforms have also been performed in Figure 3D,E and Figure S16, Supporting Information, to

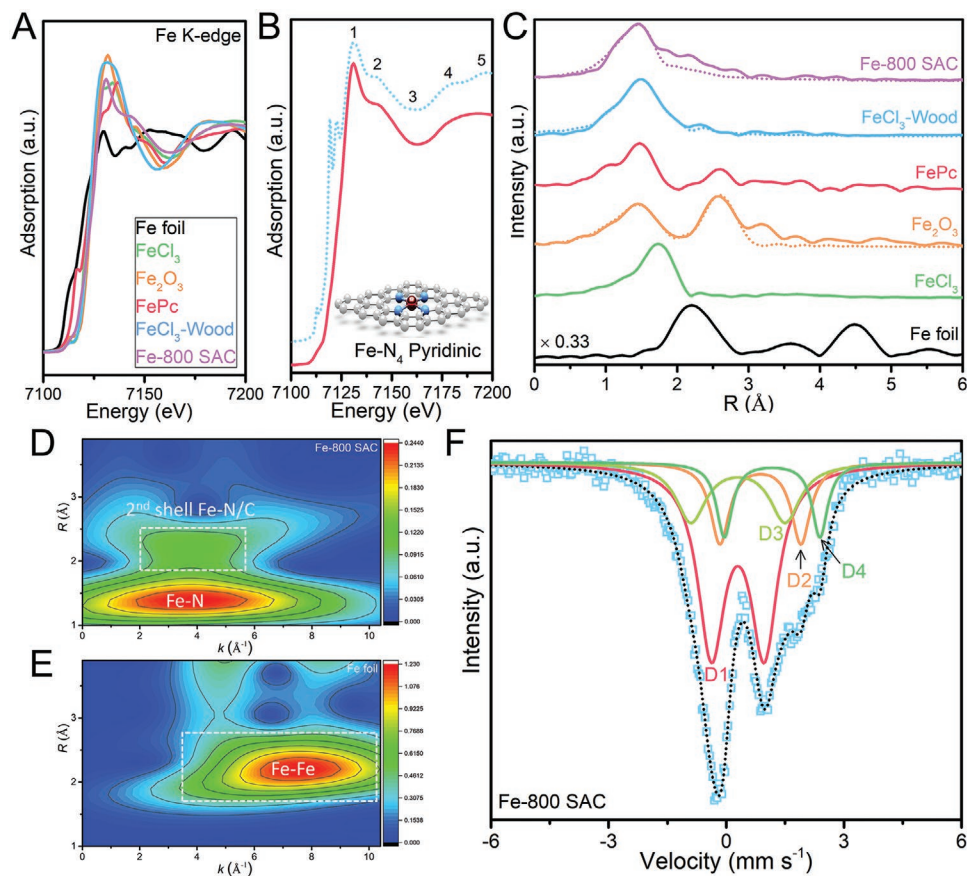


Figure 3. Coordination environment of Fe-800 SAC. A) Fe K-edge XANES spectra and B) comparison with the calculated spectrum using the pyridinic Fe–N₄ model (inset, outer carbon atoms are omitted for the sake of clarity). C) FT-EXAFS spectra of various catalysts. The dotted lines represent the FT fitting curves. D) The wavelet transform (WT) contours of Fe K-edge EXAFS spectra for Fe-800 SAC and E) Fe foil. F) Room-temperature ⁵⁷Fe Mössbauer spectrum of the ⁵⁷Fe-enriched Fe-800 SAC.

distinguish Fe–N from iron oxides. It is seen that Fe-800 SAC exhibits an intensity maximum at 3.8 Å⁻¹ from the Fe–N–C coordination but without the appearance of an Fe–Fe signal at 7.5 Å⁻¹ in Fe foil or 5.5–6.0 Å⁻¹ in iron oxides. The secondary maxima of Fe-800 SAC at 3.8 Å⁻¹ (2.2 Å in R space) is attributed to the second shell coordination of Fe–C in the proposed pyridinic Fe–N₄ structure. Control experiment without the addition of urea suggests the oxygen-containing lignins cannot stabilize the Fe single atoms upon high-temperature treatment.^[28,36]

Mössbauer spectroscopy is a powerful tool for the identification of iron species in a quantitative manner, particularly for those species with similar coordination environment but different electronic states.^[9,37,38] As shown in the room-temperature ⁵⁷Fe Mössbauer spectra in Figure 3F, Figures S17 and S18 and Table S4, Supporting Information, the proposed pyridinic Fe–N₄ coordination (53–72%, D1) is found to be dominant in all samples (except for un-pyrolyzed FeCl₃-wood with an Fe–O coordination), which is consistent with the XANES and EXAFS analysis. This D1 doublet with small isomer shift (IS, ≈0.3) and quadrupole-splitting (QS, ≈1.3) is typically assigned to the low-spin state of ferrous in the square-planar coordination (i.e., pyridinic Fe–N₄) in previous reports on the Fe–N–C catalysts.^[9] The absence of sextet and singlet in Mössbauer spectra indicate that zero-valent

metal particle is not present. Meanwhile, small fractions of other high-spin (Fe²⁺ with S = 2, D2/D4 doublets) and middle-spin (Fe²⁺ or Fe³⁺ with S = 1 or 3/2, D3 doublet) species are observed in the Fe SACs. The relatively large QS values in two high-spin species indicate a complicated coordination environment of Fe–N₄ analogues with one or two axial ligands to form a deformed octahedral structure.^[37]

2.2. Oxidative Cyclization to Synthesize Multifunctional Quinolines

As mentioned above, the hierarchically porous structure in our carbon-based SACs maximizes the exposure of active sites to reactants.^[26,33] We chose the simple oxidative dehydrogenation of tetrahydroquinoline (THQ) as a model reaction, which has been previously promoted by other SAC catalysts.^[39,40] As shown in Figure S19(A), Supporting Information, nearly quantitative conversion of THQ and above 85% selectivity of quinoline could be obtained using Fe-800 SAC at 120 °C for 48 h, which is slightly lower than the benchmark performance of 10% Pd/C. The oxidative efficiency varies significantly with the nature of transition metals. The replacement of Fe by Co further improved the selectivity to ≈100%, while Ni-800 SAC and

Cu-800 SAC gave poor or even no performance. The use of commercial 10% Fe/C, Fe₂O₃, or FeCl₃ failed to oxidize THQ due to the absence of activation site for O₂.^[41] This was further confirmed by a survey of various Fe-, Co-, and Ni-based catalysts where only SACs exhibited reactivity toward oxidative dehydrogenation (except for 10% Pd/C, CoCl₂, and cobalt ferrocene (CoFc)). Control experiments revealed that both catalyst and oxidant (O₂) are essential for this transformation.^[42] The yield of quinoline is also proportional to the catalyst loading. More importantly, we observed a strong dependence of catalytic activity on the pyrolysis temperature of Fe, Co, and Ni SACs in Figure S19, Supporting Information. This indicates that the coordination environment has strong influence on catalytic performance, which can be regulated by the replacement of four-coordinated N atoms with one or two C atoms, together with Fe aggregations at higher pyrolysis temperatures

as indicated in the EXAFS spectra in Figures S20 and S21, Supporting Information.^[36,43] The different chemical environment of doped N species at various pyrolysis temperature may give rise to differing catalytic activity, as reported in previous studies.^[44] However, regardless of the pyrolysis temperatures, we obtained closely similar pyridinic structure of Fe-SACs, as judged from FT-IR spectra, Raman spectra, SSNMR, XRD, and XPS characterizations of the Fe-SACs in Figures S11–S13, Supporting Information.

In view of the difficulty in accessing THQ subunits, a more practical approach using readily available substrates would be more attractive for the synthesis of complex, valuable quinolines.^[13,14] As shown in Figure 4A, a three-component, oxidative cyclization reaction employing feedstock chemicals aniline, acetophenone and dimethyl sulfoxide (DMSO) as the starting materials was pursued.^[15] The formation of the desired product

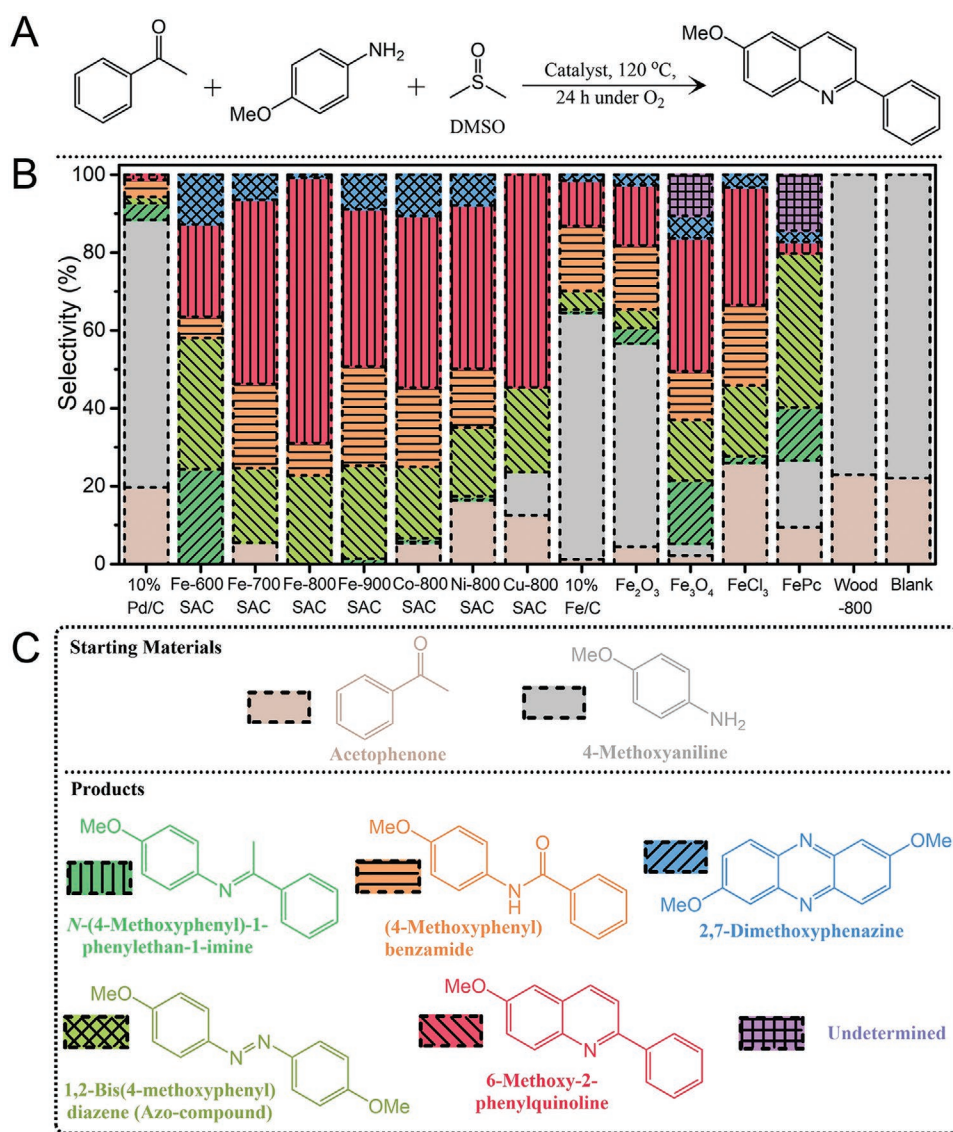


Figure 4. Oxidative cyclization toward the synthesis of quinoline. A) Model reaction of the three-component quinoline synthesis. B) Catalyst screening on the selectivity toward quinoline synthesis (in red), and C) chemical structures of starting materials and possible products. Selectivity was analyzed by GC-MS.

(6-methoxy-2-phenylquinoline) together with possible side products (imine and amide from aldol condensation as well as azo-compound and phenazine from the homo-coupling of arylamine) were monitored by gas chromatography-mass spectrometry (GC-MS) in Figure 4A. As illustrated in Figure 4B and Figure S22, Supporting Information, our SACs gave the highest GC selectivity toward quinoline derivatives among all catalysts examined ($\approx 68\%$, 44%, 42%, and 54% for Fe, Co, Ni, and Cu-800 SAC with 10 mol% catalyst loading). In contrast, commercial 10% Pd/C and 10% Fe/C catalyst only generated trace amounts of quinoline (<15%), while homogeneous FeCl₃ gave a moderate selectivity of 30%. The observation that iron oxides were catalytically active (15% and 34% for Fe₂O₃ and Fe₃O₄) means that an oxidation states between +2 and +3 is beneficial for such oxidative cyclization. As shown in Table S5, Supporting Information, temperature has a profound influence on the catalytic efficiency (entries 1–6). Lowering the reaction temperature to 80 or 100 °C prevented the thermolysis of DMSO to trigger the reaction. Further elevating the temperature to 140 °C failed to improve the yield. Since DMSO is also serving as reactant, replacement by other solvents (including HCHO and methanol as alternative proton donor) will diminish the reaction activity in entries 7–11. The existence of oxygen also has a crucial role in forming the quinoline product by the oxidative dehydrogenation in a radical pathway (entries 12 and 13).^[41] Meanwhile, the use of higher loading catalysts in entries 16–18 has no significant improvement to the reaction. The reaction order of the catalyst is almost one (linear) with a much lower slope compared to THQ dehydrogenation (6.8 vs 17.5), indicating an analogous reaction pathway to that shown in Figure S23, Supporting Information. To probe the influence of porous channel on liquid-phase reactions, control experiment using our Fe-800 SAC as monolith reactor has been conducted in entry 19, where the reaction occurs with a lower yield of 39%. This indicates the mass diffusion kinetics of reactant is not restricted by the macroporous structure.^[22] Other SAC catalysts are also catalytically active as revealed in entries 20–22, suggesting the universal applicability of such reaction.

The pyrolysis temperature had a profound influence on the catalytic efficiency, where Fe-800 SAC with the typical Fe-N₄ coordination was found to be the most effective with a TOF value (0.42 h⁻¹) comparable to homogeneous catalysts for similar three-component synthesis of quinolines in Table S6, Supporting Information. The influence of coordination environment on catalytic activity^[36] can be seen from the generation of imine as an intermediate in the reaction with Fe-600 SAC, owing to insufficient activation of acetophenone. At a lower temperature of 600 °C, the Fe-O coordination in FeCl₃-wood is not be fully converted to the desired Fe-N coordination, leading to a decrease in catalytic activity.^[36,43] As far as we know, this is the first study highlighting the synthetic utility of SACs in complex three-component reactions, paving the way toward the production of high-value chemicals in an efficient, atom-economical manner. For comparison with traditional approaches, we have also verified the catalytic efficiency of Fe-800 SAC in the modified, two-component Friedländer synthesis in Figure S24, Supporting Information, where > 95% GC yield of 2-phenylquinoline was obtained.^[45]

To assess the generality of our protocol, various combinations of substituted anilines and acetophenones were examined

in Figure 5A. For instance, multifunctional quinolines with methoxy (1b), alkyl (1a and 1d), halogens (1e–1h), and methylthio (1c) moieties at the 6-position can be efficiently constructed (46–87% yield) by using the corresponding anilines. The electronic attributes had a strong influence on the outcome of reaction, where electronic-deficient anilines generally give a lower activity to form quinoline.^[15] Substituted acetophenones with synthetically valuable functionalities such as methoxy (2a), methylthio (2b), nitro (2i), nitrile (2j), halogens (2d–2g), and trifluoromethyl (2h) can be well-tolerated by this oxidative cyclization protocol (52–78% yield) regardless of the electronic attributes. Interestingly, modification at 3-position of quinoline can be realized by using propiophenone despite of a lower yield (2k, 27%). Our protocol is also applicable to those heterocycles such as pyridine (2i and 2m), furan (2n), and thiophene (2o), which is typically challenging in the Suzuki coupling owing to strong poisoning effect to the catalytically active metal centers and requires a high loading of noble metal catalysts.^[10]

The synthetic utility of Fe₁-catalyzed oxidative cyclization was further highlighted by the deuteration at the fourth position of quinoline with low-cost deuteration reagent (DMSO-d₆).^[46] Five different representative examples with methoxy-, bromo-, methylthio-, and trifluoromethyl-units at the 2- or 6-position of quinolines were examined in Figure 5B. Similarly, all of the substrates can be deuterated with similar yields to the undeuterated analogues (42–73%). Furthermore, we explored the synthesis of a Cavosonstat derivative (a F508del-CFTR mutation treatment medicine) and its 4-deuterated analogue in Figure 5C.^[47] Despite lower yields owing to the multifunctional nature of substrate and possible side reactions, the desired compounds (3a, 35%; 3a', 32%) can be obtained by a one-step, Fe₁-catalyzed cyclization rather than traditional palladium-catalyzed Suzuki coupling between specified quinoline and phenyl boronic ester.

A kinetic study was also performed in Figure 6A to provide mechanistic insights. An induction period was observed in the initial 6 hours owing to the multi-step pathway toward quinoline formation, where the intermediate (imine) was predominately detected by GC-MS during this period. Further extending the reaction period to 42 h did not result in a better yield compared with the optimized condition. Finally, the Fe-800 SAC can be recycled eight times without any decrease in conversion (>95%) and selectivity (>60%) in Figure 6B. The additional HAADF-STEM images, ⁵⁷Fe Mössbauer and EXAFS characterization in Figure 6, and Figures S25 and S26, Supporting Information, confirm the intact single-atom nature of the spent catalyst. In particular, quantitative analysis by ⁵⁷Fe Mössbauer spectrum suggests no obvious change in the catalyst composition in D1–D4 species in Table S4. ICP testing of the supernatant of reaction mixture and the recovered catalyst also confirmed no metal leaching after reaction completion.^[12]

As shown in Figure S18, Supporting Information, the pyridinic Fe-N₄ species (D1) is believed to be catalytically active toward oxidative cyclization in view of moderate activity in Fe-600/700 SAC. The high-spin species (D2 and D4) are generally inactive because of their saturated coordination. The catalytic activity is strongly correlated to the percentage of the middle-spin species (D3), where the most active Fe-800 SAC also possesses the highest content of D3 ($\approx 19\%$). This is in good agreement with selective oxidation of the C–H bond by

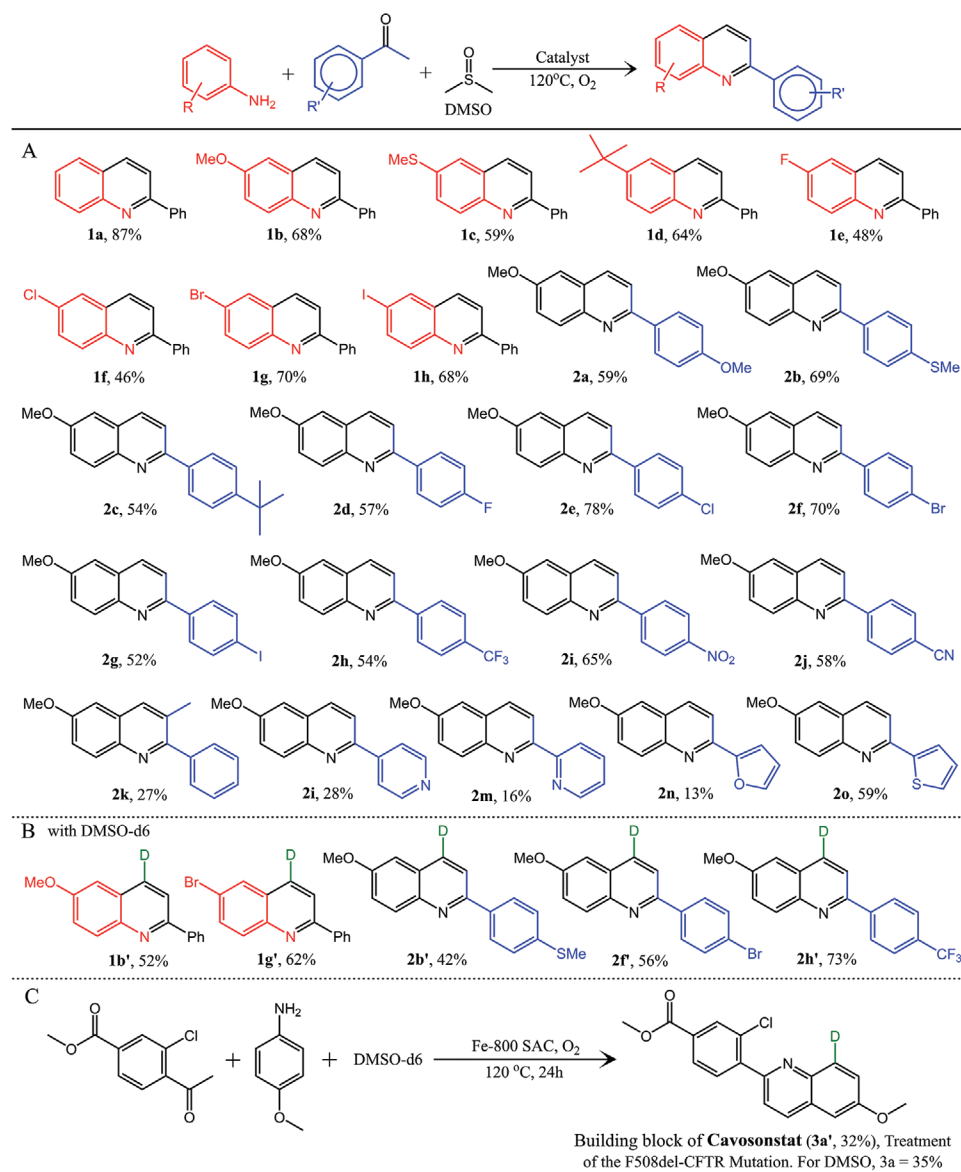


Figure 5. Synthetic utility of SAC-catalyzed oxidative cyclization. A) General reaction in the color scheme. A wide assortment of multifunctional quinolines containing halogens, nitro, nitrile, sulfides, and heterocycles can be accessed with the Fe-800 SAC catalyst. The reaction was performed with 0.1 mmol of substituted acetophenone, 0.3 mmol of substituted aniline, 10 mol% of catalyst in 1 mL of DMSO at 120 °C under O₂ for 24 h. B) Synthesis of 4-deuterated multifunctional quinolines by the same strategy with DMSO-d₆ as deuteration reagent. C) One-step synthesis of Cavosonstat building block and its 4-deuterated analogue using our Fe-800 SAC catalyst.

Fe–N–C catalyst, where the middle-spin species is 33 times more active than high-spin species and ≈ 1 order of magnitude more active than the pyridinic Fe–N₄ species.^[9] Although the detailed configuration of this middle-spin species remains unclear due to its low percentage in the Fe–N–C catalysts, they are most probably Fe²⁺ or Fe³⁺ with a spin-state of $S = 1$ or $3/2$.^[9,37,38] Considering the importance of the coordination atoms on the catalytic performance, considerable efforts have been devoted to tailor the type of coordination atoms, coordination number and second- or higher-coordination shells in recent years.^[48,49] The structure of the SAC is dynamic in the liquid phase. For instance, as demonstrated by operando ⁵⁷Fe Mössbauer spectroscopy, high-spin Fe–N₄ species suffer

from significant catalytic degradation owing to the switching of oxidation state (Fe³⁺/Fe²⁺) under ORR operating conditions in fuel cells, while the low or middle spin species are more durable and remain constant (Fe²⁺).^[50]

We have conducted DFT calculations to identify the reaction pathway of oxidative cyclization, and the influence of the coordination environment on reaction efficiency.^[40,51] Pyridinic Fe–N₄ and analogous Fe–C₁N₃, Fe–C₂N₂ structures are employed as models due to their abundance in Fe–N–C catalysts. DFT calculations and experimental evidence on the activation of O₂ by Fe–N₄ SAC and its analogues have been detailed in previous studies on the oxygen reduction reaction, benzene oxidation and oxidative dehydrogenation of THQ; these were reported to

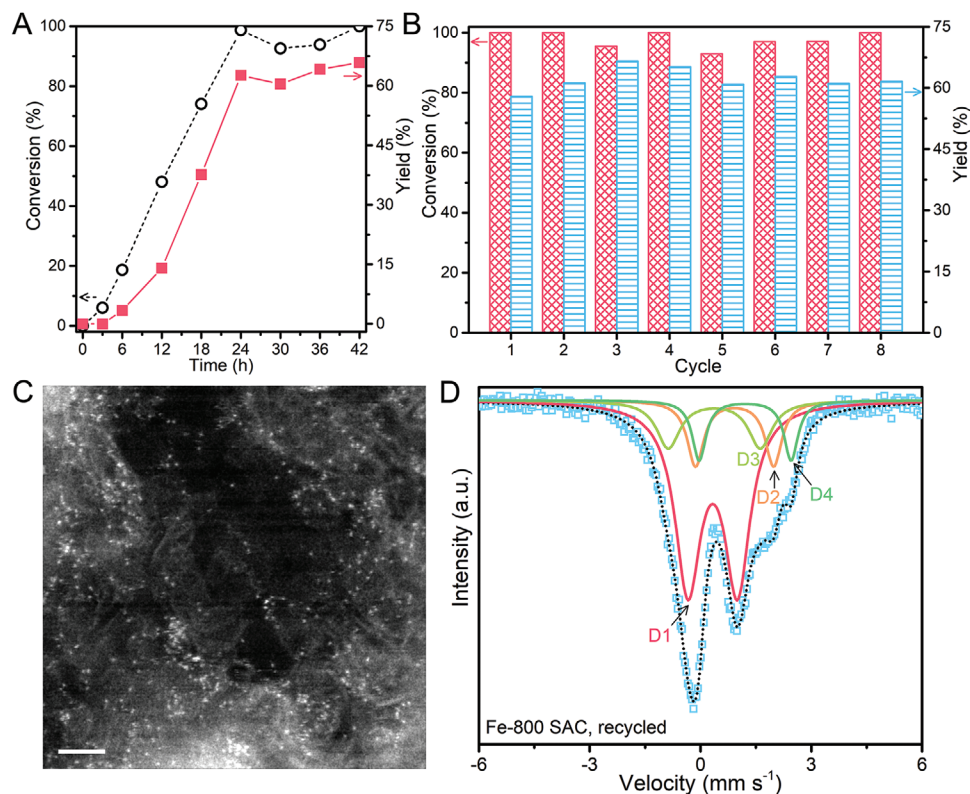


Figure 6. Kinetic study and stability measurement. A) Monitoring of the reaction under standard conditions over time. B) Cycling stability of Fe-800 SAC for the synthesis of 6-methoxy-2-phenylquinoline by oxidative cyclization. C) Atomic-resolution STEM-HAADF image of the recycled Fe-800 SAC. D) Room-temperature ^{57}Fe Mössbauer spectrum of the recycled catalyst. The reaction was performed with 0.1 mmol of acetophenone, 0.3 mmol of *p*-anisidine, 10 mol% of catalyst in 1 mL of DMSO at 120 °C under O_2 for 24 h. Scale bar: 2 nm.

follow a spin crossover pathway or a redox process involving the appearance of high-valence metal species.^[38,52] As illustrated in the proposed catalytic cycle in **Figure 7** and models in Figures S28–S30, Supporting Information, the preferred adsorption of acetophenone on metallic center is the initial step of the reaction; this is consistent with the wide substrate scope

of acetophenone regardless of its electronic attributes compared to aniline. The activation of carbonyl by SAC has been proven by Li et al. to be an exothermic step.^[53] The activated acetophenone is then reacted with the fragment of DMSO under its catalytic thermolysis to form the demethylthioated intermediate^[15] with a minimum activation barrier (≈ 0.5 eV) over the Fe-N_4 or $\text{Fe-C}_1\text{N}_3$

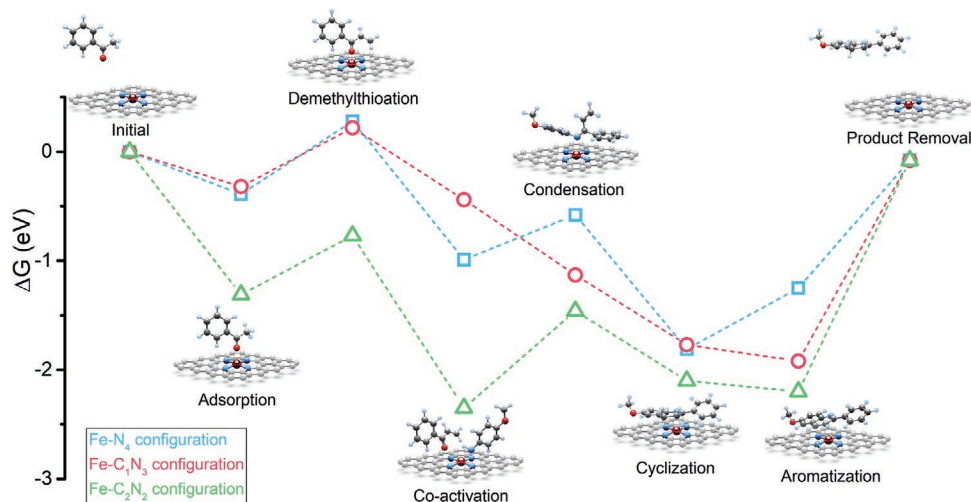


Figure 7. Proposed mechanism by DFT calculation. Energy profiles of the oxidative cyclization of acetophenone and *p*-anisidine over Fe SACs with the Fe-N_4 , $\text{Fe-C}_1\text{N}_3$, or $\text{Fe-C}_2\text{N}_2$ coordinations. Inset shows the optimized configurations of reactants, intermediates, and product on an Fe-N_4 catalyst. The color scheme used: crimson for Fe, blue for N, gray for C, red for O, and white for H. Outer carbon atoms in the model are omitted for the sake of clarity.

catalyst. A similar pathway to homogeneous catalysis may be operational, in which acetophenone reacts with sulfenium cation to form phenyl vinyl ketone, and amino group serves as proton donor to the decomposition of DMSO in the control experiments in Figure S27, Supporting Information. This further promotes the exothermic, co-activation of aniline and subsequent condensation to form the imine intermediate, which is a detectable side product in GC-MS. Such condensation process is calculated to be highly dependent on the coordination environment of the catalyst, where Fe–C₂N₂ exhibits a relatively high energy barrier (≈1 eV) compared to others. The following cyclization and aromatization to afford the quinoline structure are relatively rapid in term of thermodynamics, as-proven by the excellent performance of SACs toward the oxidative dehydrogenation of THQ in Figure S19, Supporting Information.^[39] Meanwhile, the desorption process of quinoline product from the catalyst surface is sluggish and could be rate-determining step owing to its strong π - π interaction (poisoning) with the catalyst, especially in the case of Fe–C₂N₂ and Fe–C₁N₃. This can be attributed to the charge-deficient nature of the Fe center after the replacement of N by one or two C, leading to a stronger interaction with external heteroatoms (such as, N in quinoline).^[36] Based on the above DFT calculations, we propose the Fe–N₄ coordination with lower reaction barriers would be the primarily active center for this three-component reaction.

3. Conclusion

We have successfully synthesized a mechanically strong, hierarchically porous support for SACs by immobilizing transition metal atoms (M = Fe, Co, Ni, Cu) in natural wood by a top-down pyrolysis approach. Such carbon-supported SACs exhibited excellent catalytic activities and selectivity toward the oxidative dehydrogenation of THQ, as well as, the three-component, oxidative cyclization to afford 6-methoxy-2-phenylquinoline, outperforming the benchmark Pd/C, Fe/C, and homogeneous FeCl₃ catalysts. The superior performance of our SACs is attributed to the optimized metal–N₄ coordination with relatively weak product desorption energy, as well as, maximized exposure of active sites to reactants by the hierarchically porous carbon plates.

4. Experimental Section

Synthesis of Fe₁-Single-Atom Catalysts: Natural wood sticks (birch) were purchased from Daiso (Singapore), cut into rectangular shape (5 × 1 × 0.2 cm³ along the growth direction) and dried at 100 °C for 24 h to evaporate all the moisture. Prior to use, 30 g of dried wood sticks were extracted in 225 mL of an ethanol/toluene mixture (1:2, v/v) at 75 °C for 24 h and then washed with ethanol (3 ×) and acetone (1×) before drying at 75 °C to remove unwanted waxes, fats, and resins. 14 g of extracted wood sticks were then immersed into 20 mL of a 0.05 M FeCl₃ ethanol/conc. HCl solution (4:1, v/v) in a 50 mL Teflon-lined stainless-steel autoclave. After soaking at room temperature for 2 h, the autoclave was sealed and heated at 140 °C for 2 h in an oven and then cooled down to room temperature naturally. (Caution: Corrosive ethanol/conc. HCl mixture was used and the hydrothermal temperature should not

go beyond 140 °C) Hydrothermal treated wood sticks were taken out, thoroughly washed by water, ethanol until the supernatant became colorless and dried at 80 °C overnight before soaking into an urea aqueous solution for another 24 h. After that, 14 g of FeCl₃/urea treated wood sticks were loaded into a quartz boat (20 × 10 × 2 cm³), transferred to a tube furnace under 50 sccm of Ar gas, and then heated to 800 °C at 5 °C min⁻¹ and maintained for 2 h. The Fe loading on carbonized wood (≈0.8 wt%) was determined by ICP-OES. The Fe loading can be further increased to ≈2.5 wt% by using 0.5 M FeCl₃ ethanol/conc. HCl mixture, respectively. In the case of Co₁, Ni₁, or Cu₁-SACs, a 0.05 M CoCl₂, NiCl₂, or CuCl₂ ethanol/conc. HCl mixture were used. Control samples without the addition of FeCl₃ or urea were also prepared.

Oxidative Dehydrogenation of Tetrahydroquinoline Using Fe₁-Single-Atom Catalyst: Typically, Fe₁-SAC (5 mol% Fe) was loaded in a vial with 2 mL of mesitylene, 0.1 mmol of 1,2,3,4-tetrahydro-quinoline (THQ, 12.55 μL) and stirred at 120 °C for 48 h in air.^[39] After reaction, the solid catalyst was recovered by centrifugation and washed with ethyl acetate for 3 times. The organic substance was combined and concentrated under reduced pressure. After completely removal of mesitylene by evaporation, the crude product was analyzed by GC-MS.

The Construction of Substituted Quinolines by Oxidative Cyclization Using Fe₁-Single-Atom Catalysts: Typically, Fe-800 SAC (10 mol% Fe) was loaded in Schlenk tube with 1 mL of DMSO, 0.1 mmol of acetophenone (11.66 μL), and 0.3 mmol of *p*-anisidine (37.96 mg). The mixture was stirred at 120 °C for 24 h under O₂ atmosphere (O₂ balloon).^[15] After reaction, the solid catalyst was recovered by centrifugation and washed with ethyl acetate for 3 times. 10 mL of brine was added to the organic substance, and the resulting mixture was extracted with 5 mL of ethyl acetate (3×). The combined organic layer was washed with 10 mL of brine for another 3 cycles and dried over anhydrous Na₂SO₄. After completely removal of ethyl acetate by evaporation, the crude product was analyzed by GC-MS. To obtain the 4-deuterated derivatives, 1 mL of DMSO-d₆ was used with other identical conditions. For stability measurement, the solid catalyst was recovered by centrifugation and thoroughly washed by DMSO, ethyl acetate and dried at 80 °C overnight before re-dispensing for another cycle.

Material Characterization: The following equipment was used: STEM (JEOL ARM200F equipped with ASCOR probe corrector at 80 kV), SEM (JEOL JSM-6701F), TEM (JEM 2010F, 200 kV), XPS (AXIS UltraDLD, monochromatic Al K_α), XRD (Bruker D8), TGA (Discovery 5500), ICP-OES (Perkin Elmer Avio 500, ppm level accuracy), GC-MS (Agilent 5975 C inert MSD with triple-axis detector), MS (Bruker MicroTOF-QII), NMR (Bruker AV400), BET (Quantachrome Instruments Autosorb-iQ, 77K), Raman (WITec Alpha 300R), FT-IR (Bruker vertex 80v), SSNMR (9T Bruker Advance Neo 400 MHz, wide-bore, 4 mm probe). XANES/EXAFS: SAC samples were cut into a dimension of 1 × 1 cm² and placed onto sample holder. Measurements were carried out at the Singapore Synchrotron Light Source, X-ray Absorption Fine Structure for Catalysis beamline.^[54] Data analysis and simulation were carried out on Athena, Artemis, and Hephaestus (Version 0.9.23).^[55]

Room-Temperature ⁵⁷Fe Mössbauer Spectroscopy: ⁵⁷Fe-enriched samples were prepared by dissolving 100 mg of ⁵⁷Fe foil (Isoflex) in 4.2 mL of concentrated HCl, 3.4 mL of water, and 1.0 mL of 30% H₂O₂ with stirring at 75 °C until complete dissolution. 4.8 mL of the above ⁵⁷FeCl₃ clear solution was added to 16 mL of ethanol for the hydrothermal treatment of raw wood at 140 °C for 2h. ⁵⁷Fe-enriched SACs were prepared by soaking in urea solution, drying, and subsequent annealing at various temperatures. The ⁵⁷Fe Mössbauer measurements were performed with a proportional counter and a Topologic 500A spectrometer with ⁵⁷Co (Rh) as a γ ray radioactive source. An Fe foil was used to calibrate the velocity.

Supporting Information

Supporting Information is available from the Wiley Online Library or from the author.

Acknowledgements

K.P.L. acknowledges NRF-CRP grant “Two-Dimensional Covalent Organic Framework: Synthesis and Applications,” grant number NRF-CRP16-2015-02, funded by National Research Foundation, Prime Minister’s Office, Singapore. X.P. would like to thank the National Science Foundation of China (31971614, 21736003), Guangdong Natural Science Funds for Distinguished Young Scholar (2016A030306027), Guangdong Natural Science Funds (2017A030313130), Guangzhou Science and Technology Funds (201904010078), State Key Laboratory of Pulp and Paper Engineering and Fundamental Research Funds for the Central Universities. J.W. would like to thank the International Partnership Program of Chinese Academy of Sciences (No. 121421KYSB 20170020). The authors appreciate the near-edge X-ray adsorption measurement by Dr. Caozheng Diao at Singapore Synchrotron Light Source (SSLS), Soft X-ray—ultraviolet (SUV) beamline and the SSNMR measurement by Dr. Gustavo G. Shimamoto at NUS CMMAC Laboratories.

Conflict of Interest

The authors declare no conflict of interest.

Author Contributions

Z.C. and J.S. contributed equally to this work. Z.C. and J.S. conceived the research, synthesized the materials, conducted catalytic reactions, and wrote the draft under the supervision of X.P. and K.P.L. TEM, STEM characterization, and data analysis were conducted by Z.C., X.Z., and X.Z.; X-ray adsorption measurements and data processing were conducted by S.X.; Mössbauer spectra and data analysis were performed by W.Z., R.G., A.I.R., and J.W.; SEM measurements were conducted by J.S. and R.L.; X.P. and L.Z. performed the XPS measurements; J.L., R.L., C.L., H.X., H. L., L.W., X.L., and M.J.K. assisted with materials characterization and data analysis. All authors discussed and commented on the manuscript.

Data Availability

The data that support the findings of this study are available from the corresponding author upon reasonable request.

Keywords

hierarchically porous structure, organic catalysis, oxidative cyclization, single-atom catalysts, three-component reaction

Received: February 18, 2021

Revised: May 1, 2021

Published online:

- [1] A. Wang, J. Li, T. Zhang, *Nat. Rev. Chem.* **2018**, *2*, 65.
- [2] X. Cui, W. Li, P. Ryabchuk, K. Junge, M. Beller, *Nat. Catal.* **2018**, *1*, 385.
- [3] Y. Pan, C. Zhang, Z. Liu, C. Chen, Y. Li, *Matter* **2020**, *2*, 78.
- [4] H. Yan, C. Su, J. He, W. Chen, *J. Mater. Chem. A* **2018**, *6*, 8793.
- [5] L. Zhang, Y. Ren, W. Liu, A. Wang, T. Zhang, *Natl. Sci. Rev.* **2018**, *5*, 653.
- [6] L. Liu, M. Lopez-Haro, C. W. Lopes, C. Li, P. Concepcion, L. Simonelli, J. J. Calvino, A. Corma, *Nat. Mater.* **2019**, *17*, 866.

- [7] L. Lin, S. Yao, R. Gao, X. Liang, Q. Yu, Y. Deng, J. Liu, M. Peng, Z. Jiang, S. Li, Y.-W. Li, X.-D. Wen, W. Zhou, D. Ma, *Nat. Nanotechnol.* **2019**, *14*, 354.
- [8] Y. Zhu, W. Sun, J. Luo, W. Chen, T. Cao, L. Zheng, J. Dong, J. Zhang, M. Zhang, Y. Han, C. Chen, Q. Peng, D. Wang, Y. Li, *Nat. Commun.* **2018**, *9*, 3861.
- [9] W. Liu, L. Zhang, X. Liu, X. Liu, X. Yang, S. Miao, W. Wang, A. Wang, T. Zhang, *J. Am. Chem. Soc.* **2017**, *139*, 10790.
- [10] Z. Chen, E. Vorobyeva, S. Mitchell, E. Fako, M. A. Ortuño, N. López, S. M. Collins, P. A. Midgley, S. Richard, G. Vilé, J. Pérez-Ramírez, *Nat. Nanotechnol.* **2018**, *13*, 702.
- [11] C. Liu, Z. Chen, H. Yan, S. Xi, K. M. Yam, J. Gao, Y. Du, J. Li, X. Zhao, K. Xie, H. Xu, X. Li, K. Leng, S. J. Pennycook, B. Liu, C. Zhang, M. J. Koh, K. P. Loh, *Sci. Adv.* **2019**, *5*, eaay1537.
- [12] Z. Chen, C. Liu, J. Liu, J. Li, S. Xi, X. Chi, H. Xu, I.-H. Park, X. Peng, X. Li, W. Yu, X. Liu, L. Zhong, K. Leng, W. Huang, M. J. Koh, K. P. Loh, *Adv. Mater.* **2020**, *32*, 1906437.
- [13] J. Marco-Contelles, E. Pérez-Mayoral, A. Samadi, M. d. C. Carreiras, E. Soriano, *Chem. Rev.* **2009**, *109*, 2652.
- [14] V. V. Kouznetsov, L. Y. V. Méndez, C. M. M. Gómez, *Curr. Org. Chem.* **2005**, *9*, 141.
- [15] Y. Liu, Y. Hu, Z. Cao, X. Zhan, W. Luo, Q. Liu, C. Guo, *Adv. Synth. Catal.* **2018**, *360*, 2691.
- [16] S. Mahato, A. Mukherjee, S. Santra, G. V. Zyryanov, A. Majee, *Org. Biomol. Chem.* **2019**, *17*, 7907.
- [17] S. M. Prajapati, K. D. Patel, R. H. Vekariya, S. N. Panchal, H. D. Patel, *RSC Adv.* **2014**, *4*, 24463.
- [18] L.-H. Li, Z.-J. Niu, Y.-M. Liang, *Chem. - Asian J.* **2020**, *15*, 231.
- [19] L. Liu, A. Corma, *Chem. Rev.* **2018**, *118*, 4981.
- [20] Y. Yang, Y. Yang, Z. Pei, K.-H. Wu, C. Tan, H. Wang, L. Wei, A. Mahmood, C. Yan, J. Dong, S. Zhao, Y. Chen, *Matter* **2020**, *3*, 1442.
- [21] T. Li, Y. Zhai, S. He, W. Gan, Z. Wei, M. Heidarinejad, D. Dalgo, R. Mi, X. Zhao, J. Song, J. Dai, C. Chen, A. Aili, A. Vellore, A. Martini, R. Yang, J. Srebric, X. Yin, L. Hu, *Science* **2019**, *364*, 760.
- [22] Y. Wang, G. Sun, J. Dai, G. Chen, J. Morgenstern, Y. Wang, S. Kang, M. Zhu, S. Das, L. Cui, L. Hu, *Adv. Mater.* **2017**, *29*, 1604257.
- [23] A. Husbands, S. Cranford, *Matter* **2019**, *1*, 1092.
- [24] Z.-L. Yu, N. Yang, L.-C. Zhou, Z.-Y. Ma, Y.-B. Zhu, Y.-Y. Lu, B. Qin, W.-Y. Xing, T. Ma, S.-C. Li, H.-L. Gao, H.-A. Wu, S.-H. Yu, *Sci. Adv.* **2018**, *4*, eaat7223.
- [25] S. Mitchell, N.-L. Michels, J. Pérez-Ramírez, *Chem. Soc. Rev.* **2013**, *42*, 6094.
- [26] X. Peng, L. Zhang, Z. Chen, L. Zhong, D. Zhao, X. Chi, X. Zhao, L. Li, X. Lu, K. Leng, C. Liu, W. Liu, W. Tang, K. P. Loh, *Adv. Mater.* **2019**, *31*, 1900341.
- [27] Z. Chen, H. Zhuo, Y. Hu, H. Lai, L. Liu, L. Zhong, X. Peng, *Adv. Funct. Mater.* **2020**, *30*, 1910292.
- [28] Y. Ohashi, T. Watanabe, *ACS Omega* **2018**, *3*, 16271.
- [29] H. Zhou, S. Hong, H. Zhang, Y. Chen, H. Xu, X. Wang, Z. Jiang, S. Chen, Y. Liu, *Appl. Catal., B* **2019**, *256*, 117767.
- [30] W. Chen, X.-W. Peng, L.-X. Zhong, R.-C. Sun, *ACS Sustainable Chem. Eng.* **2015**, *3*, 1366.
- [31] Y. Huang, Y. Chen, X. Fan, N. Luo, S. Zhou, S.-C. Chen, N. Zhao, C. P. Wong, *Small* **2018**, *14*, 1801520.
- [32] J. Sun, S. E. Lowe, L. Zhang, Y. Wang, K. Pang, Y. Wang, Y. Zhong, P. Liu, K. Zhao, Z. Tang, H. Zhao, *Angew. Chem., Int. Ed.* **2018**, *57*, 16511.
- [33] Z. Chen, C. Liu, X. Zhao, H. Yan, J. Li, P. Lyu, Y. Du, S. Xi, K. Chi, X. Chi, H. Xu, X. Li, W. Fu, K. Leng, S. J. Pennycook, S. Wang, K. P. Loh, *Adv. Mater.* **2019**, *31*, 1804763.
- [34] Z. Chen, K. Leng, X. Zhao, S. Malkhandi, W. Tang, B. Tian, L. Dong, L. Zheng, M. Lin, B. S. Yeo, K. P. Loh, *Nat. Commun.* **2017**, *8*, 14548.

- [35] J. Meng, J. Li, J. Liu, X. Zhang, G. Jiang, L. Ma, Z.-Y. Hu, S. Xi, Y. Zhao, M. Yan, P. Wang, X. Liu, Q. Li, J. Z. Liu, T. Wu, L. Ma, *ACS Cent. Sci.* **2020**, *6*, 1431.
- [36] Y. Pan, Y. Chen, K. Wu, Z. Chen, S. Liu, X. Cao, W.-C. Cheong, T. Meng, J. Luo, L. Zheng, C. Liu, D. Wang, Q. Peng, J. Li, C. Chen, *Nat. Commun.* **2019**, *10*, 4290.
- [37] U. I. Kramm, M. Lefèvre, N. Larouche, D. Schmeisser, J.-P. Dodelet, *J. Am. Chem. Soc.* **2014**, *136*, 978.
- [38] X. Li, C.-S. Cao, S.-F. Hung, Y.-R. Lu, W. Cai, A. I. Rykov, S. Miao, S. Xi, H. Yang, Z. Hu, J. Wang, J. Zhao, E. E. Alp, W. Xu, T.-S. Chan, H. Chen, Q. Xiong, H. Xiao, Y. Huang, J. Li, T. Zhang, B. Liu, *Chem* **2020**, *6*, 3440.
- [39] S. Wei, Y. Wang, W. Chen, Z. Li, W.-C. Cheong, Q. Zhang, Y. Gong, L. Gu, C. Chen, D. Wang, Q. Peng, Y. Li, *Chem. Sci.* **2020**, *11*, 786.
- [40] Y. Han, Z. Wang, R. Xu, W. Zhang, W. Chen, L. Zheng, J. Zhang, J. Luo, K. Wu, Y. Zhu, C. Chen, Q. Peng, Q. Liu, P. Hu, D. Wang, Y. Li, *Angew. Chem., Int. Ed.* **2018**, *57*, 11262.
- [41] D. Xu, H. Zhao, Z. Dong, J. Ma, *ChemCatChem* **2019**, *11*, 5475.
- [42] J. Li, G. Liu, X. Long, G. Gao, J. Wu, F. Li, *J. Catal.* **2017**, *355*, 53.
- [43] Y.-N. Gong, L. Jiao, Y. Qian, C.-Y. Pan, L. Zheng, X. Cai, B. Liu, S.-H. Yu, H.-L. Jiang, *Angew. Chem., Int. Ed.* **2020**, *59*, 2705.
- [44] J. Zhang, C. Zheng, M. Zhang, Y. Qiu, Q. Xu, W.-C. Cheong, W. Chen, L. Zheng, L. Gu, Z. Hu, D. Wang, Y. Li, *Nano Res.* **2020**, *13*, 3082.
- [45] K. Motokura, T. Mizugaki, K. Ebitani, K. Kaneda, *Tetrahedron Lett.* **2004**, *45*, 6029.
- [46] T. Pirali, M. Serafini, S. Cargnin, A. A. Genazzani, *J. Med. Chem.* **2019**, *62*, 5276.
- [47] K. W. Southern, S. Patel, I. P. Sinha, S. J. Nevtitt, *Cochrane Database Syst. Rev.* **2018**, *8*, 1465.
- [48] J. Yang, W. Li, D. Wang, Y. Li, *Small Struct.* **2021**, *2*, 2000051.
- [49] X. Li, H. Rong, J. Zhang, D. Wang, Y. Li, *Nano Res.* **2020**, *13*, 1842.
- [50] J. Li, M. T. Sougrati, A. Zitolo, J. M. Ablett, I. C. Oğuz, T. Mineva, I. Matanovic, P. Atanasov, Y. Huang, I. Zenyuk, A. Di Cicco, K. Kumar, L. Dubau, F. Maillard, G. Dražić, F. Jaouen, *Nat. Catal.* **2021**, *4*, 10.
- [51] L. Wang, M.-X. Chen, Q.-Q. Yan, S.-L. Xu, S.-Q. Chu, P. Chen, Y. Lin, H.-W. Liang, *Sci. Adv.* **2019**, *5*, eaax6322.
- [52] H.-T. Lien, S.-T. Chang, P.-T. Chen, D. P. Wong, Y.-C. Chang, Y.-R. Lu, C.-L. Dong, C.-H. Wang, K.-H. Chen, L.-C. Chen, *Nat. Commun.* **2020**, *11*, 4233.
- [53] L. Kuai, Z. Chen, S. Liu, E. Kan, N. Yu, Y. Ren, C. Fang, X. Li, Y. Li, B. Geng, *Nat. Commun.* **2020**, *11*, 48.
- [54] Y. Du, Y. Zhu, S. Xi, P. Yang, H. O. Moser, M. B. H. Breese, A. Borgna, *J. Synchrotron Radiat.* **2015**, *22*, 839.
- [55] B. Ravel, M. Newville, *J. Synchrotron Radiat.* **2005**, *12*, 537.